Available online at www.sciencedirect.com
SCIENCE DIRECT
Electrochimica Acta 51 (2006) 4680–4692
ELECTROCHIMICA Acta
www.elsevier.com/locate/electacta

High performance polymer electrolyte fuel cells with ultra-low Pt loading electrodes prepared by dual ion-beam assisted deposition

Madhu Sudan Saha [a], Andrea F. Gullá [b], Robert J. Allen [b], Sanjeev Mukerjee [a,*,1]

[a] *Department of Chemistry and Chemical Biology, Northeastern University, 360 Huntington Ave, Boston, MA 02115, USA*
[b] *E-TEK Division of De Nora North America, Inc., Somerset, NJ 08873, USA*

Received 27 December 2005; accepted 2 January 2006
Available online 3 February 2006

Abstract

Ultra-low pure Pt-based electrodes (0.04–0.12 mg_{Pt}/cm^2) were prepared by dual ion-beam assisted deposition (dual IBAD) method on the surface of a non-catalyzed gas diffusion layer (GDL) substrate. Film thicknesses ranged between 250 and 750 Å, these are compared with a control, a conventional Pt/C (1.0 $mg_{Pt(MEA)}/cm^2$, E-TEK). The IBAD electrode constituted a significantly different morphology, where low density Pt deposits (largely amorphous) were formed with varying depths of penetration into the gas diffusion layer, exhibiting a gradual change towards increasing crystalline character (from 250 to 750 Å). Mass specific power density of 0.297 g_{Pt}/kW is reported with 250 Å IBAD deposit (0.04 mg_{Pt}/cm^2 for a total MEA loading of 0.08 mg_{Pt}/cm^2) at 0.65 V. This is contrasted with the commercial MEA with a loading of 1 $mg_{Pt(MEA)}/cm^2$ where mass specific power density obtained was 1.18 g_{Pt}/kW (at 0.65 V), a value typical of current state of the art commercial electrodes containing Pt/C. The principal shortcoming in this effort is the area specific power density which was in the range of 0.27–0.43 W/cm^2 (for 250–750 Å IBAD) at 0.65 V, hence much below the automotive target value of 0.8–0.9 W/cm^2 (at 0.65 V). An attempt to mitigate these losses is reported with the use of patterning. In this context a series of patterns ranging from 45 to 80% Pt coverage were used in conjunction with a hexagonal hole geometry. Up to 30% lowering of mass transport losses were realized.

Keywords: Low Pt loading; Dual IBAD; PEMFC; Electrode kinetics; Oxygen reduction reaction

1. Introduction

The proton exchange membrane fuel cells (PEMFCs) are a highly attractive power source for vehicular and stationary applications due to its many advantages compared with other fuel cell systems [1–3]. As one might realize, the use of Pt-based catalyst represents one of the main limitations of the technology in terms of its commercial viability. In the last decade, much of the developmental work has been focused on ways to improve the performance of polymer electrolytes, electrocatalyst, and electrode materials [4,5] while decreasing the amount of precious metal present in the system. Cost saving can be gained through several approaches such as reducing electrocatalyst loading and by achieving a more effective three-phase electrolyte–catalyst–gas phase boundary, thus leading to better catalyst utilization. The introduction of supported platinum on carbon blacks has already helped lower the platinum loadings of PEMFC's from several mg_{Pt}/cm^2 to about 0.4–0.5 mg_{Pt}/cm^2 [6,7]. Researchers at Los Alamos National Laboratories [6,7] were able to bring the cathode platinum loading down to 0.12 mg_{Pt}/cm^2 with no detrimental effect on fuel cell performance. In parallel to this, efforts at Texas A&M University also exhibited great strides towards lowering Pt loadings as low as 0.05 mg_{Pt}/cm^2 with comparable performance to those previously reported with 5 mg_{Pt}/cm^2 [8,9]. In a recent report on activity benchmarks and future requirements for electrocatalysts in the context of PEM fuel cells, Gasteiger et al. [10] have pointed out that for automotive application the current state of the art (with H_2/air at 80 °C), which is at approximately 0.7 W/cm^2 at 0.68 V (for 58% energy conversion) corresponding to 0.85–1.1 g_{Pt}/kW requires to transition to 0.2 g_{Pt}/kW at $\geq$ 0.65 V. This can be envisaged as a duel effort wherein (a) MEA power density is improved to 0.8–0.9 W/cm^2_{MEA} at $\geq$ 0.65V by increasing Pt utilization and lowering mass transport and ohmic contributions and (b) increasing the inherent activities of the

* Corresponding author. Tel.: +1 617 373 2382; fax: +1 617 373 8949.
E-mail address: s.mukerjee@neu.edu (S. Mukerjee).
[1] ISE member.

0013-4686/$ – see front matter © 2006 Elsevier Ltd. All rights reserved.
doi:10.1016/j.electacta.2006.01.006

reaction zone by changing the nature of the conventional supported Pt electrocatalysts (Pt nanoparticles) via means such as alloying and modification of surface morphology. In this context it is important to note that the noble metal loading at the anode can be reduced from the current loadings of 0.2–0.4 to 0.05 $mg_{Pt(MEA)}/cm^2$ without concomitant losses at the anode [11]. Hence the principal effort in this context involves the cathode electrode.

At the current state of the technology, prior efforts together with current approaches have to be tempered with ability to translate developments in this regard to mass manufacturability keeping reproducibility (batch versus continuous) and cost in perspective. Depending on the deposition methods used, the approach towards lowering noble metal loading can be classified into four broad categories: (i) thin film formation with carbon supported electrocatalysts, (ii) pulse electrodeposition of noble metals (Pt and Pt alloys), (iii) sputter deposition (iv) pulse laser deposition and (v) ion-beam deposition. While the principal aim in all these efforts is to improve the charge transfer efficiency at the interface, it is important to note that while some of these approaches provide for a better interfacial contact allowing for efficient movement of ions, electrons and dissolved reactants in the reaction zone, others additionally effect modification of the electrocatalyst surface (such as those rendered via sputtering, electrodeposition or other deposition methods).

In the first of the four broad categories using the 'thin film' approach in conjunction with conventional carbon supported electrocatalysts, several variations have been reported, these include (a) the so called 'decal' approach where the electrocatalyst layer is cast on a PTFE blank and then decaled on to the membrane [12,13]. Alternatively an 'ink' comprising of Nafion® solution, water, glycerol and electrocatalyst is coated directly on to the membrane (in the Na^+ form) [14]. These catalyst coated membranes are subsequently dried (under vacuum, 160 °C) and ion exchanged to the H^+ form [14]. Modifications to this approach have been reported with variations to choice of solvents and heat treatment [15,16] as well as choice of carbon supports with different microstructure [17]. Other variations to the 'thin film' approach have also been reported such as those using variations in ionomer blends [18], ink formulations [19], spraying techniques [20,21], pore forming agents [22], and various ion exchange processes [23]. At its core this approach relies on extending the reaction zone further into the electrode structure away from the membrane, thereby providing for a more three dimensional zone for charge transfer. Most of the variations reported above thereby enable improved transport of ions, electrons and dissolved reactant and products in this 'reaction layer' motivated by need to improve electrocatalyst utilization. These attempts in conjunction with use of Pt alloy electrocatalysts have formed the bulk of the current state of the art in the PEM fuel cell technology. Among the limitations of this approach are problems with controlling the Pt particle size (with loading on carbon in excess of 40%), uniformity of deposition in large scale production and cost (due to several complex processes and/or steps involved).

An alternative method for enabling higher electrocatalyst utilization has been attempted with pulse electrodeposition. Taylor et al. [24], one of the first to report this approach used pulse electrodeposition with Pt salt solutions which relied on their diffusion through thin Nafion® films on carbon support enabling electrodeposition in regions of ionic and electronic contact on the electrode surface. See a recent review on this method by Taylor et al., describing various approaches to pulse electrodeposition of catalytic metals [25]. In principal this methodology is similar to the 'thin film' approach described above, albeit with a more efficient electrocatalyst utilization, since the deposition of electrocatalysts theoretically happens at the most efficient contact zones for ionic and electronic pathways. Improvements to this approach have been reported such as by Antoine and Durand [26] and by Popov [27]. Developments in the pulse algorithms and cell design have enabled narrow particle size range (2–4 nm) with high efficiency factors and mass activities for oxygen reduction. Though attractive, there are concerns on the scalability of this method for mass scale manufacturing.

Sputter deposition of metals on carbon gas diffusion media is another alternative approach. Here however interfacial reaction zone is more in the front surface of the electrode at the interface with the membrane. The original approach in this case was to put a layer of sputter deposit on top of a regular Pt/C containing conventional gas diffusion electrode. Such an approach [28] exhibited a boost in performance by moving part of the interfacial reaction zone in the immediate vicinity of the membrane. Recently, Hirano et al. [29] reported promising results with thin layer of sputter deposited Pt on wet proofed non-catalyzed gas diffusion electrode (equivalent to 0.01 mg_{Pt}/cm^2) with similar results as compared to a conventional Pt/C (0.4 mg_{Pt}/cm^2) electrode obtained commercially. Later Cha and Lee [30], have used an approach with multiple sputtered layers (5 nm layers) of Pt interspersed with Nafion®-carbon-isopropanol ink (total loading equivalent of 0.043 mg_{Pt}/cm^2) exhibiting equivalent performance to conventional commercial electrodes with 0.4 mg_{Pt}/cm^2. Huag [31] studied the effect of substrate on the sputtered electrodes. Further, O'Hare et al., on a study of the sputter layer thickness has reported best results with a 10 nm thick layer. Further, significant advancements have been made with sputter deposition as applied to direct methanol fuel cells (DMFC) by Witham et al. [32,33], wherein several fold enhancements in DMFC performance was reported compared to electrodes containing unsupported PtRu catalyst. Catalyst utilization of 2300 mW/mg at a current density of 260–380 mA/cm^2 was reported [32,33]. While the sputtering technique provides for a cheap direct deposition method, the principal drawback is the durability. In most cases the deposition has relatively poor adherence to the substrate and under variable conditions of load and temperature, there is a greater probability of dissolution and sintering of the deposits.

An alternative method dealing direct deposition was recently reported using pulsed laser deposition [34]. Excellent performance was reported with loading of 0.017 mg_{Pt}/cm^2 in a PEMFC, however this was only with the anode electrodes, no cathode application has been reported to date.

However, in all these new direct deposition methodologies, mass manufacturability with adequate control on reproducibility remains questionable at best. In this regard the methodologies developed by 3M company is noteworthy, where mass manufacture of electrodes with low noble metal loading is reported [35,36]. Here a series of vacuum deposition steps are involved with adequate selection of solvents and carbon blacks resulting in nanostructured noble metal containing carbon fibrils which are embedded into the ionomer–membrane interface [37,38].

An alternative is the use of ion-beam techniques, where the benefits of low energy ion bombardment concurrent to thin film vacuum deposition (electron beam) process is exploited for achieving dense, adhering and robust depositions [39]. This method has been recently reviewed [39] in terms of both mechanisms of ion/solid interactions during thin film growth as well as development of various protocols for specific application areas, including tribology, anti corrosion coatings, superconducting buffer layers and coatings on temperature sensitive substrates such as polymers. Modifications of this approach to prepare 3D structures including overhang and hollow structures have also been recently reported [40]. Use of dual anode ion source for high current ion-beam applications has also been reported recently [41], where benefits for mass production environment is discussed.

It is the objective of this work to present an improved deposition methodology based on ion deposition technique which overcomes many of the limitations previously presented and able to produce a Pt electrode having (i) better utilization of the precious metal present on the electrode in PEMFCs and (ii) very low precious metal (Pt) loading. Moreover, the deposition methodology used has the advantage of being a low temperature process and very easy to scale up. This technique allows producing a catalyst entirely composed of metal nanoparticles/nanocrystalline thin film with control in size and distribution, while eliminating the need for dispersing and supporting medium. In another area, IBAD gas diffusion electrodes (GDE's) have the potentiality to create highly customized products therefore also revolutionizing the micro fuel cells market.

The gas diffusion electrode is prepared by direct metallization (via IBAD) of non-catalyzed gas diffusion layer (GDL). In our recent previous communication in this regard [42], we have reported PEM fuel cell performance with dual ion-beam electrodes having very low precious metal loading (0.04–0.12 mg_{Pt}/cm^2, corresponding to a deposition of 250 and 750 Å Pt deposits) exhibiting relatively high fuel cell PEMFC performance. The fuel cell performance of electrode assemblies (with Nafion® 112 used as proton conducting membrane) with a total membrane electrode assembly (MEA) Pt loading of 0.24 mg_{Pt}/cm^2 compared to 1 mg_{Pt}/cm^2 exhibited a three-fold mass activity enhancement for a comparison at 850 mV for a PEMFC operating with 50/60 psig anode and cathode back pressure, respectively, in H_2/O_2 at 80 °C. Here we report details of the electrode morphology and correlate it to PEMFC performance in the context of its commercial application.

2. Experimental

2.1. Electrode preparation by dual ion-beam assisted deposition technique

Dual IBAD is a vacuum-deposition process that combines physical vapor deposition (PVD) with ion-beam bombardment. Vapor of coating atoms are generated with an electron-beam evaporator and deposited on a substrate. Ions are simultaneously extracted from the plasma and accelerated into the growing PVD film at energies of several hundred to several thousand electronvolts (500–2000 eV). Ion bombardment is the key factor controlling film properties in the IBAD process; thus imparting substantial energy to the coating and coating/substrate interface. This achieves the benefits of substrate heating (which generally provides a denser, more uniform film) without degrading its bulk properties. The major parameters of the process are coating material, evaporation-rate, ion species, ion energy and ion-beam current density described in details elsewhere [43–45]. In this work, dual IBAD was used to directly deposit onto a commercially available non-catalyzed GDL (LT1400, E-TEK) a layer of pure Pt with pre-chosen deposition thicknesses of 250, 550 and 750 Å. The total metal deposited on the GDL had a loading in the range between 0.04 and 0.12 mg_{Pt}/cm^2; thus forming a very thin layer of catalyst with a low precious metal loading, hereafter referred to as gas diffusion electrode (GDE). In the attempt to further improve the catalyst utilization and gas/liquid diffusivity of the IBAD prepared electrodes, a set of patterned depositions were also used. The patterns were based on a simple honeycomb design which had been chemically etched into a rigid frame. The frame was secured on top of the GDL and the deposition was carried on as usual. The patterns had different transparencies (fraction of void space) in the range of zero to 55%. The GDL consisted of a three dimensional woven web structure comprised of a carbon cloth support, as a substrate with a coating of Teflonized-carbon (Vulcan-XC 72, Cabot Corp., USA) providing for a matrix with a gas diffusion layer (LT1400). Such a GDL also improved tensile properties and surface roughness which is perfectly suited for superficial metal deposition obtained through IBAD. Comparison was made with respect to a conventional electrodes containing supported Pt/C (anode and cathode side), 0.5 mg_{Pt}/cm^2 (each electrode, total MEA loading of 1 mg_{Pt}/cm^2 precious metal) with conventional 30% Pt/C electrocatalysts (commercial electrodes from E-TEK, a division of De Nora North America, Somerset, NJ). The choice of the current GDL (LT1400, E-TEK) was based on the fact that this serves as the substrate for the current state of the art reaction layer containing the Pt/C commercial electrocatalysts (E-TEK, 30% Pt on C) which was used as the control, therefore eliminating effects of the substrate layers in the comparison. The current GDL (LT1400) therefore is by no means optimized for the IBAD deposition; this is an ongoing effort in our current endeavors.

2.2. Preparation of the membrane and electrode assembly

The membrane electrode assembly (MEA) was prepared using a Nafion® 112 membrane (DuPont). Prior to MEA fab-

rication, the membrane was cleaned by immersing in boiling 3% H_2O_2 for 1 h followed by boiling 1 M H_2SO_4 for the same duration with subsequent rinsing in boiling deionized water (1 h). This procedure was repeated at least twice to ensure complete removal of H_2SO_4. The MEA was fabricated in-house via hot pressing (100 °C < T < 130 °C, 5 min < t < 10 min and 125 psig < P < 250 psig). Contrary to the conventional MEA assemblies, no extra liquid ionomer was used in the MEA fabrication involving the IBAD electrodes.

2.3. Assembly of the single cell and its installation in the test station

All MEAs were tested in a 5 cm^2 single cell fuel cell (Fuel Cell Technologies, Albuquerque, NM) using a standard fuel cell test station (built in-house) designed to carry out steady-state polarization measurements. This cell allowed for simultaneous measurements of both single and half cell data with the aid of reference electrodes in the anode chamber (hydrogen reference). The fuel cell test station also allows independent control of humidification, cell temperature and gas flow rate. All MEAs were conditioned prior to testing using a series of steps; the initial step involved a so-called "break-in" process in which the cell temperature is slowly raised (approximately 20 °C/h) from ambient temperature to the operational point under N_2. After keeping the cell under these conditions for approximately 5 h in order to allow proper conditioning of the MEA assembly, the pressure was slowly increased to 50/60 psig (anode/cathode, respectively). The gases were then switched to saturated H_2 and air/O_2 and the cell was allowed to equilibrate for a couple of hours. Steady state polarization was measured using a three-electrode mode potentiostatically with the aid of an electronic load (Agilent® model 6050A) and in-house Labview® (National Instruments) software program. The program enabled measurement of current after reaching a steady state within a window of fluctuations. Adjustment of conditions was made such that the forward and reverse polarizations exhibited negligible hysteresis, an essential condition for proper steady state measurements. This was further confirmed by separately polarizing the electrode at set potentials and following the current variations for periods up to 1200 min.

Cyclic voltammetry was conducted at room temperature using an Autolab potentiostat/galvanostat (Model, PGSTAT-30, Ecochemie, Brinkman Instruments). The electrodes, in a completely flooded configuration were cycled both in the presence and absence of CO in 1 M $HClO_4$. For CO stripping voltammetry, pure CO was purged closed to the working electrode for at least 1 h with the electrode polarized at 0.05 V versus RHE in a fume hood. The electrode was then purged with pure N_2 for 1 h under potential control followed by voltammetric stripping. All cyclic voltammetric experiments were recorded between 0.05 and 1.2 V with a scan rate of 20 mV/s.

The morphological characterization of the electrodes was conducted using SEM/EDAX technique (Hitachi Field Emission SEM/EDAX, model number 5800 with Genesis model 136-10 EDAX containing Z-max window for lighter elements). The scanning electron microscope image was observed at different points along the electrode, top surface and lateral cross-section. For the lateral cross-section a microtome (Reidhert ultra-cut model # E with a diamond knife) with 0.5 μm section size was used.

3. Results and discussion

To avoid confusion between the various terminologies used in the text, the gas diffusion layer (GDL) refers to the non-catalyzed diffuser (LT1400-W, E-TEK) as described in the previous section. The terminology gas diffusion electrode (GDE) will refer to the IBAD prepared electrodes (IBAD GDE); whenever needed the various thickness of the IBAD GDE's will be clearly pointed out, e.g. IBAD250 corresponds to the electrode having a 250 Å thick Pt layer deposited directly onto the non-catalyzed diffuser, the same is valid for the remaining two electrodes; IBAD550 equal to 550 Å layer and IBAD750 equal to 750 Å layer. The loadings corresponding to each of the three different thickness electrodes prepared via IBAD are the following 0.04 mg_{Pt}/cm^2 (IBAD250), 0.08 mg_{Pt}/cm^2 (IBAD550) and finally 0.12 mg_{Pt}/cm^2 (IBAD750). Thus when preparing an MEA, the total precious metal loading will be the one obtained by adding the cathodic and anodic sides of the cell (e.g. the MEA comprised of the IBAD250 will have a total precious metal loading of about 0.08 mg_{Pt}/cm^2). In the case of the patterned IBAD electrodes, the best fuel cell performance was obtained with the 70% transparency (or 70% Pt coverage) having a precious metal loading of 0.084 mg_{Pt}/cm^2 (IBAD750P).

3.1. Morphologies of IBAD GDE

Fig. 1 shows the SEM micrographs taken for non-catalyzed GDL (Fig. 1a) and after metallization, the IBAD750 GDE (Fig. 1b) with a magnification of 50,000 times. The top surface of the gas diffusion layer is covered by the Pt deposited layer. From the micrographs it emerges that no change in the surface morphology of carbon support is observed i.e., intrinsic porous structure of the gas diffusion layer remains practically unchanged after metallization. This is evident from a comparison of Fig. 1a and b. This is very important from the perspective of mass transport of dissolved reactants to the IBAD deposits (reaction centers) and the removal of water at the cathode electrode. Further Fig. 1c shows the nature of these IBAD deposits from the perspective of the electrode cross-section as represented by 250, 550 and 750 Å deposits. From these cross-sections, it is seen that the depositions are primarily limited to the top surface of the GDL with an evident increase in thickness of the deposits between 250 and 750 Å. It is important to note however that there is a difference between these cross-sections and the designated deposition thickness (250–750 Å). The cross-sections indicate the depth of the deposit into the non-catalyzed porous electrode structure (GDL), whereas the designated deposition thickness such as 250 Å is the thickness of the deposit on top of the carbon surface. This depth of deposit into the electrode structure is further confirmed using EDAX spectrum of the IBAD GDE (Fig. 1d) which reveals an increase of the deposition thickness, this includes both an increase of the depth of penetration into

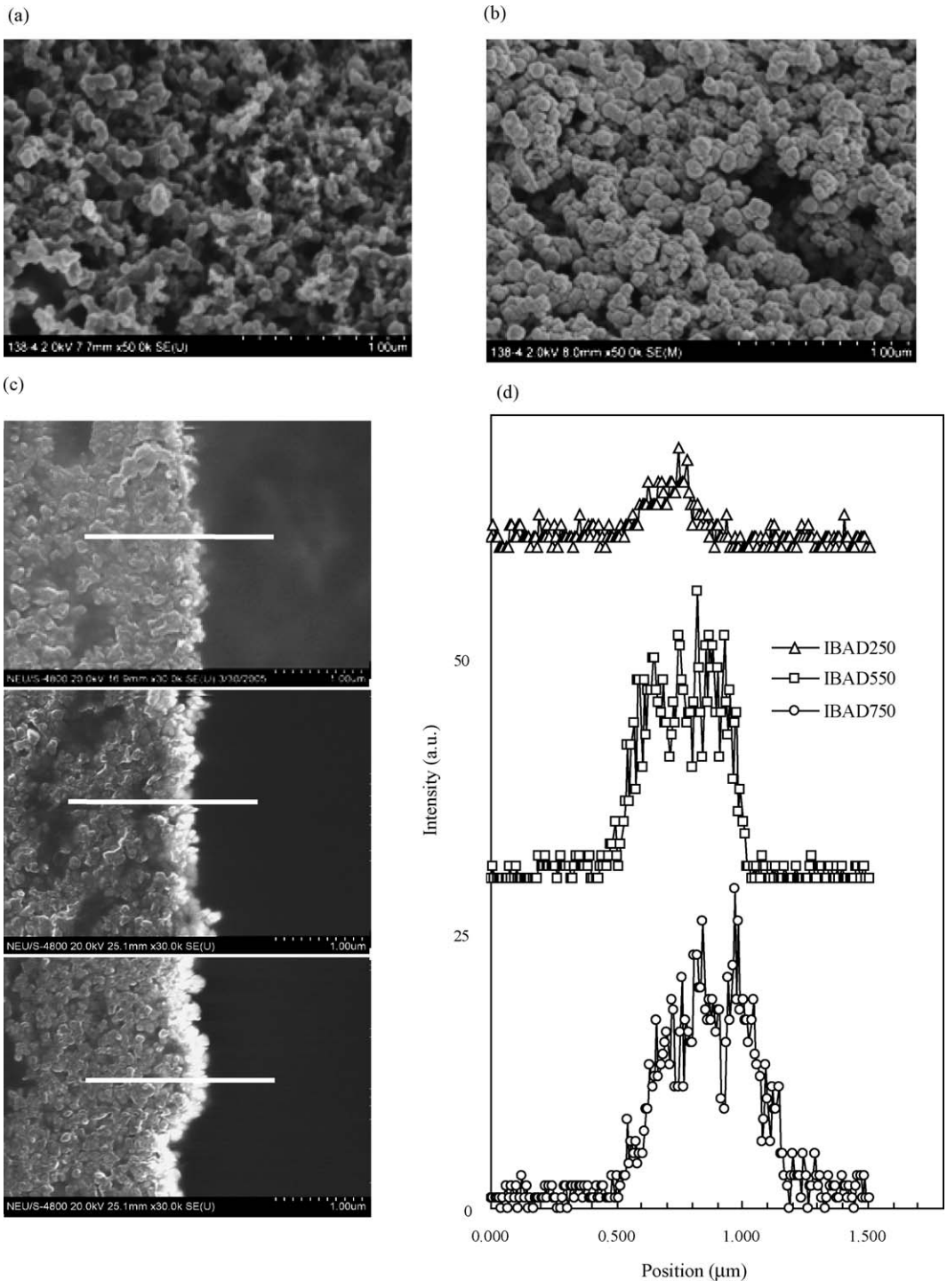

Fig. 1. (a) SEM micrograph of the non-catalyzed GDL (LT1400) compared to (b) corresponding micrograph of the IBAD250 having an electrode loading of 0.04 mg_{Pt}/cm^2. (c) Cross-section SEM images of the IBAD GDE's (750, 550 and 250 Å deposits). Note that the Pt deposits are represented by the lighter contrast in the SEM pictures. (d) EDAX profile of the IBAD GDEs along the line in (c) showing the depth of deposit on the GDL electrode.

the GDL structure and an increase of the density of Pt at the top surface. From the weight of Pt deposited and its depth, it is easy to calculate the density of Pt. Based on the EDAX spectrum, the density of Pt located at the top surface of the GDL exhibits an increase from 0.10 to 1.72 g/cm^3 going from 250 to 750 Å. It is important to note that the bulk density of Pt is 21.45 g/cm^3. Hence these constitute a largely amorphous nano-phasic deposit.

The X-ray diffraction patterns for the IBAD GDE's and a standard E-TEK GDE are shown in Fig. 2. Judging from the features represented by (1 1 1) diffraction peak ($2\Theta = 39.764^\circ$) and using the peak width at half intensity (Scherrer treatment), the crystallite size is estimated at 9–10 nm for IBAD GDE which is larger than typically encountered in supported Pt/C where the range of particle sizes are 2.5–4 nm. The X-ray patterns shown

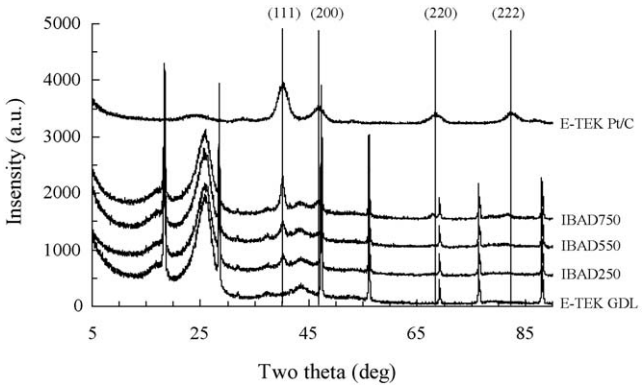

Fig. 2. XRD patterns of the non-catalyzed GDL (LT1400) compared to the IBAD electrodes (IBAD250, IBAD550 and IBAD750 having precious metal loadings of 0.04, 0.08 and 0.12 mg_{Pt}/cm^2, respectively). Note the gradual emergence of principal diffraction peaks for Pt represented by (1 1 1), (2 0 0), (2 2 0) and (2 2 2). A representative XRD profile of a Pt/C commercial electrocatalyst (30% on carbon) is included for reference.

in Fig. 2 clearly indicate that increased loading results in gradual increase in crystallinity which is evident from the gradual emergence of extra diffraction lines such as those in (2 2 0) and (2 2 2). This increased crystalline character with higher deposition is also manifest in the increased Pt density described earlier based on EDAX results.

3.2. CO_{ads} stripping voltammetry

Stripping voltammetry of adsorbed CO (CO_{ads}) can yield useful in situ electrochemical information about Pt-based catalyst surfaces in the electrochemical environment [46,47]. This method involves the adsorption of CO on the catalyst surface at negative potentials and the oxidation of the CO_{ads} to CO_2 in a subsequent positive potential scan. Fig. 3a shows adsorbed CO_{ads} stripping scans for the IBAD GDE's in the flooded electrode (1 M $HClO_4$) mode. CO was purged while holding the potential at 0.05 V versus RHE for 1 h at 25 °C. The roughness factor (r_f) and the real Pt surface (A_{Pt}, m^2/g_{Pt}) from CO_{ads} stripping were measured using the following equations [47]:

$$r_f\,(cm^2/cm^2) = \frac{Q_{CO_{ads}}}{420\,\mu C\,cm^{-2}} \quad (1)$$

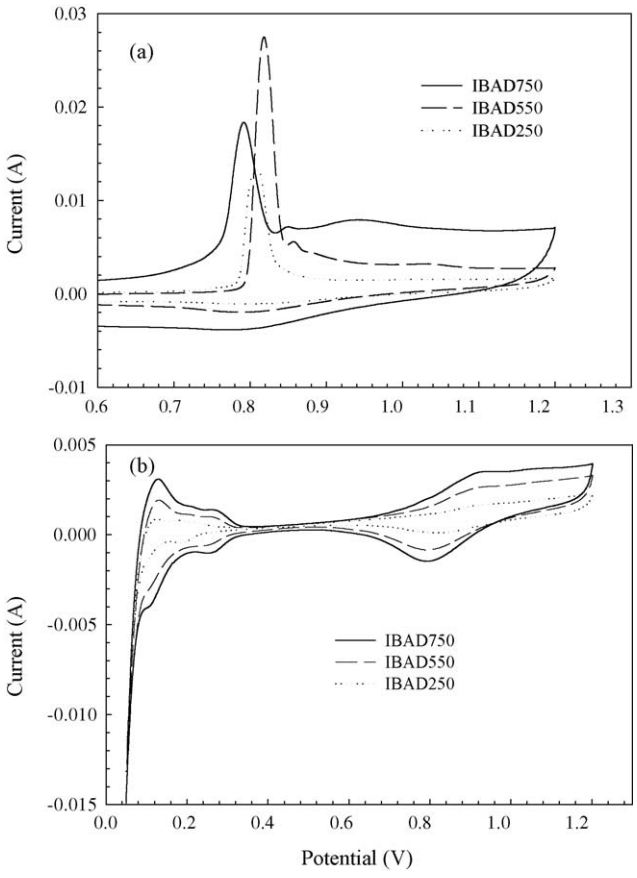

Fig. 3. Cyclic voltammograms of IBAD GDEs (a) in the presence and (b) absence of CO in 1 M $HClO_4$ at room temperature. Potential scan rate: 20 mV/s. The CO was absorbed at 0.05 V for 1 h, subsequently, the solution CO was removed by N_2 bubbling for 1 h while maintaining the potential at 0.05 V vs. RHE.

$$A_{Pt}\,(m^2/g_{Pt}) = \frac{r_f}{\text{Pt loading}} \quad (2)$$

The electrochemically active surface area of the IBAD GDE's was also estimated from the integrated charge in the hydrogen adsorption and desorption region of the CVs. The calculated values of roughness factors (cm^2/cm^2) as well as roughness factors normalized on the basis of Pt loading (cathode electrode) are listed in Table 1. In this case 220 $\mu C/cm^2$ were used for the oxidation of atomic hydrogen, a typical value based on smooth Pt

Table 1
PEMFC Tafel kinetic parameters for oxygen reduction obtained from a series of IBAD electrodes ranging in Pt deposition thickness between 750 and 250 Å corresponding to Pt loading variation in the range of 0.12–0.04 mg_{Pt}/cm^2

Electrode	E_0 (mV)	b (mV/decade)	$I_{900\,mV}$ (mA/cm^2)	$I_{900\,mV}$ (mA/mg_{Pt})	S_{EL}[a] (cm^2/cm^2)	A_{EL}[b] (m^2/g_{Pt})
IBAD250	1006	71.1	35.8	894.7	15.9 (14.5)	39.7 (36.3)
IBAD550	1010	68.5	59.8	747.8	20.3 (18.1)	25.4 (22.6)
IBAD750	1027	65.7	84.2	701.9	26.7 (21.6)	22.3 (18.0)
Std. E-TEK[c]	1021	56.8	135.2	270.4	158.1 (145.2)	31.6 (29.1)

Values from a representative standard Pt/C commercial (E-TEK, De Nora, NJ) electrode (0.5 mg_{Pt}/cm^2) is shown. These values correspond to a cell operating condition of 80 °C, Nafion® 112 membrane, 50/60 psig anode and cathode back pressure, H_2/O_2. Also shown are the corresponding roughness factors obtained using CO_{ads} stripping voltammetry and from the H_{ads}/H_{des} regions of the voltammograms. The corresponding mass specific surface areas are also shown (m^2/g_{Pt}).

[a] S_{EL}: real surface area obtained electrochemically, the values in bracket is obtained from the average of hydrogen adsorption/desorption peaks.

[b] A_{EL}: real surface area obtained electrochemically per gram of catalyst, the values in brackets are those obtained using hydrogen adsorption/desorption region.

[c] 0.5 mg/cm^2 Nafion® loading on electrode.

surface. Comparison of roughness factors (cm^2/cm^2) and mass specific surface areas (m^2/g) obtained from CO_{ads} and H_{upd} indicate remarkable agreement. In the literature there is a very wide variation of mass specific surface areas for conventional Pt/C electrocatalysts which according to recent review [10] ranges from 20 to 120 m^2/g. Our data of 31.6 m^2/g is in the lower end of the spectrum. In the case of IBAD, the roughness factors are significantly lower as compared to conventional Pt/C electrocatalysts (approximately 85%), a difference attributed to the IBAD surface morphology. The roughness factor also changes linearly with the IBAD deposition thickness, with a smooth variation between 750 and 250 Å, with a corresponding lowering of roughness factor to the extent of ~30–35%. However the mass specific surface areas (m^2/g, Table 1), are close to the conventional Pt/C electrocatalysts, in fact the IBAD250 has a higher value, close to 40 m^2/g. The comparison of the CO_{ads} stripping peaks (Fig. 3a) shows distinct differences between IBAD750 to the other IBAD electrodes (250 and 550 Å), in fact a shift in onset of CO_{ads} stripping to the extent of 45 mV is observed. However a lower dense and more amorphous deposit in the 550 and 250 Å could be attributed to this shift, this is also indicative of changes in the surface properties for the deposits below 750 Å. A careful comparison of the oxide formation and reduction peaks in Fig. 3b indicates a similar shift between 750 Å and those corresponding to 250 and 550 Å. Hence the shift in the onset of CO desorption appears to be a result of a concomitant shift towards more positive potentials in the oxide formation for the more amorphous (and less dense) 250 and 550 Å deposits. However a comparison of the H_{ads}/H_{des} peaks shows lesser distinctions (Fig. 3b).

3.3. Single-cell performance

Fig. 4a and b shows the single cell performance of H_2/O_2 and H_2/air showing the effect of Nafion® loading on the electrode surface. Polarization characteristics were compared at 80 °C with 50/60 psig backpressure for the anode and cathode electrodes, respectively (100% humidification condition). The MEAs were made with IBAD250, anode and cathode GDE's. The overall fuel cell performance of the MEA loaded with 0.5 mg/cm^2 Nafion® solution is clearly lower relative to the performance of the same MEA without Nafion®. At a fixed potential of 0.7 V, the cell performance of Nafion® coated IBAD250 MEA was 180 mA/cm^2 while the corresponding performance without Nafion® was 430 mA/cm^2; thus showing a drop in current density of about 250 mA/cm^2 for the former case. In order to

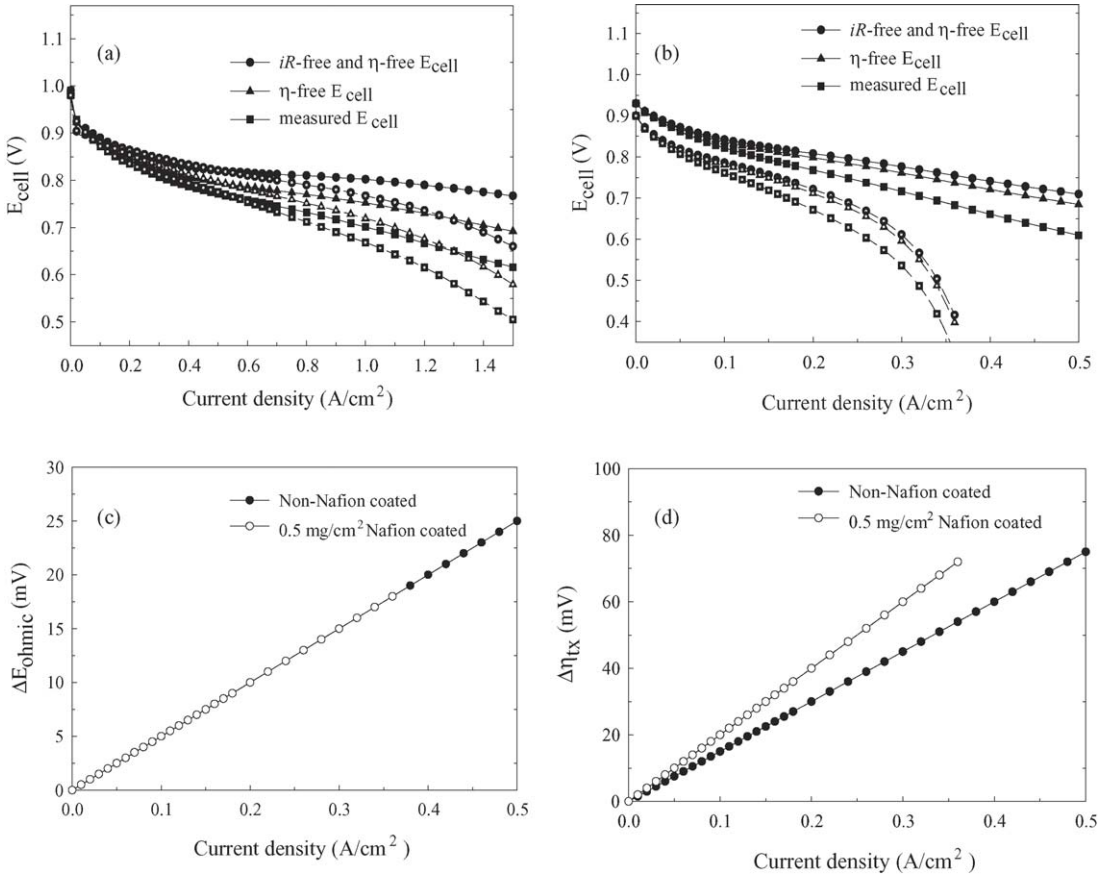

Fig. 4. Single cell performance with MEA's containing IBAD250 (0.08 $mg_{Pt(MEA)}/cm^2$) as anode and cathode electrodes showing (a) H_2/O_2 and (b) H_2/air performance with (- - -) and without out (—) 0.5 mg/cm^2 Nafion® loading on the electrode. Membrane used was Nafion® 112, other operating parameters include, 50/60 psig anode and cathode back pressure, 80 °C (cell temperature) and the stoichiometric ratios (at 1 A/cm^2) were 4.5 H_2 and 3.5 air. Relative contribution from the polarization losses due to activation, ohmic and mass transport is shown. Comparison of (c) ohmic polarization losses, ΔE_{ohmic} and (d) mass-transport losses, $\Delta\eta_{tx}$ as a function of current density are shown.

understand the true significance of the effect of Nafion® loading on the electrode performance it is important to examine its effect in all the polarization regions corresponding to the activation, ohmic and mass transport. The following equation will be used to analyze the fuel cell performance data [10,48]:

$$E_{\text{cell}} = E_{\text{rev}(P_{H_2}, P_{O_2}, T)} - \Delta E_{\text{ohmic}} - \eta_{\text{ORR}} - \eta_{\text{tx}} \quad (3)$$

The first term on the right-hand side of Eq. (3) is the reversible H_2/O_2 cell voltage, which depends on the partial pressures of the reactants and the cell temperature, the corresponding value based on the experimental conditions is 1.169 V. ΔE_{ohmic} is the ohmic voltage loss which can be measured directly via either current-interrupt or high-frequency resistance measurements. η_{ORR} is the so-called cathode overpotential losses and η_{tx} is the mass-transport overpotential losses. The parameter η_{tx} was evaluated by a non-linear least-square fit of Eq. (3) to the experimental data for the both H_2/O_2 and H_2/air. The relative ohmic overpotential losses for both Nafion® loaded and non-Nafion® IBAD electrodes were found to be identical while the contribution from mass-transport overpotential losses for the Nafion® loading IBAD electrode was very significant, as shown in Fig. 4d. The fact that a non-Nafion® loaded GDE performed better is significant as it reduces a significant step in the MEA manufacturing step. Further it also indicates that the different morphology of the electrocatalyst at the electrode-membrane interface requires a more careful analysis of transport in the substrate GDL (LT1400 non-catalyzed layer, E-TEK).

The electrocatalytic layer of the standard E-TEK GDE (0.5 mg_{Pt}/cm^2) was loaded with a Nafion® solution of 0.5 mg/cm^2, this is a typical Nafion® loading used in our MEA's when conventional carbon supported electrocatalysts are used. The polarization of this commercial Pt/C containing MEA was compared to MEA containing IBAD750 electrodes, measured in the same test fixture as the IBAD GDE cells and subject to same test conditions and protocols and the performances of the two MEAs are compared in Fig. 5. As shown in the comparison with H_2/O_2, IBAD and Pt/C electrodes show relatively small difference in the low current density activation controlled region (Fig. 5a). An *iR*-corrected Tafel plot of the performance in H_2/O_2 shows the expected variation based on the difference of Pt loading (0.24 mg_{Pt}/cm^2 in IBAD 750 mg_{Pt}/cm^2 versus 1 mg_{Pt}/cm^2 for Pt/C electrode). Assuming no increase in the mass-transport losses as the Pt loading is reduced, the change in cell voltage as a function of cathode Pt loading can be described mathematically

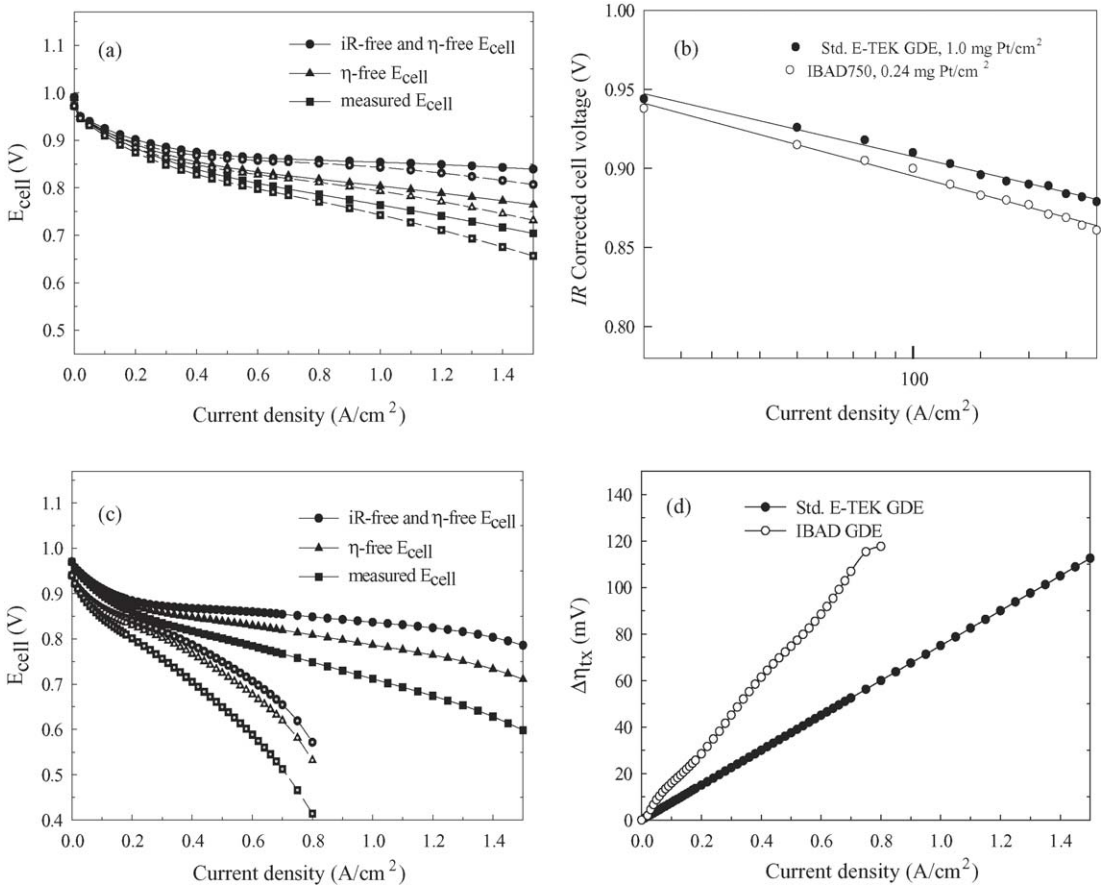

Fig. 5. Comparison of cell performance with MEA's made comprising of IBAD750 GDE (0.24 $mg_{Pt(MEA)}/cm^2$) (- - -) as anode and cathode electrodes and standard E-TEK GDE (LT140E-W; 1.0 $mg_{Pt(MEA)}/cm^2$) (—) for (a) H_2/O_2 at 80 °C Nafion® 112 membrane, 50/60 psig anode and cathode back pressure and the stoichiometric ratios (at 1 A/cm^2) were 4.5 H_2 and 3.5 air. The corresponding *iR*-corrected Tafel plot is shown in (b) comparing activation polarization characteristics. (c) Corresponding H_2/air operation showing the relative contributions of all three polarizations losses (activation, ohmic and mass transport). (d) Mass-transport losses, $\Delta\eta_{\text{tx}}$ is shown as a function of current density for better comparison.

on the basis of the known O_2 reduction kinetics [48]:

$$\left.\frac{\delta E}{\delta \log[L_{ca}]}\right|_{P_{O_2},P_{H_2},T,i} = -b \quad (4)$$

where L_{ca} denotes the cathode Pt loading. Eq. (4) states that the change in cell voltage with the logarithm of the cathode Pt loading (assuming the same catalyst is used) is proportional to the Tafel-slope. For a Tafel-slope of 70 mV/decade at 80 °C, a loading reduction by a factor of 2 or 4 is thus predicted leading to voltage loss across the entire current density range of ≈20 or ≈40 mV, respectively. In our comparison, this assumption can be expected to hold till the end of the ohmic controlled region. At 200 mA/cm^2, the *iR*-corrected potential difference between the two is approximately 20 mV, this is on the lower side based on the above equation. However as assumed in Eq. (4), this difference relies on comparison of similar electrocatalysts with different loading, whereas, in our case a comparison is between a nanoparticle and a thin layer (largely amorphous) coating with significantly different surface morphology.

Comparison at higher current density, especially in H_2/air (Fig. 5c) shows that the MEA made with E-TEK electrodes exhibit higher performance as compared to the IBAD750 MEA. The main contributing factor responsible for the lower performance of the IBAD MEA is O_2 deprivation due to flooding as evidenced from significantly higher mass-transport losses in the case of IBAD750 electrode compared to the E-TEK GDE (Fig. 5d). A similar analysis comparing ohmic overpotentials showed negligible differences (not shown).

As mentioned in the introduction section, recent review by Gasteiger et al. [10] has pointed out that one of the yardsticks for PEM fuel cell performance in terms of targets for automotive use is the need to transition from the current state of the art of approximately 0.7 W/cm^2 (at 0.65 V, for a conversion efficiency of 55%) corresponding to a Pt-specific power density of 0.85–1.1 g_{Pt}/kW. This is the performance we obtain with H_2/air at 80 °C (full humidification) using Pt/C commercial electrodes from E-TEK (Table 2). This value is clearly far above the target value (for automotive application) of <0.2 g_{Pt}/kW at ≥0.65 V (for 55% energy conversion), translating to a target of area specific power density in the range of 0.8–0.9 W/cm$^2_{MEA}$ at ≥0.65 V. While a considerable amount of this improvement can be realized by improving the electrocatalyst utilization, significant breakthroughs are necessary in the activation overpotential.

Under condition of H_2/air feed at 80 °C, the MEA made with IBAD750 GDE (0.24 $mg_{Pt(MEA)}$/cm^2) resulted in power density of 0.327 W/cm^2 at 0.65 V, translating into a Pt-specific power density of 0.734 g_{Pt}/kW (Table 2 and Fig. 5c). Hence while the area specific power density is lower the gravimetric power density is improved. The lower area specific power density for IBAD MEA as compared to E-TEK GDE is due to the higher mass-transport induced voltage losses for the former case (Fig. 5d). As shown in Fig. 5d, the difference between the two is to the extent of ∼50% at 0.65 V. It is therefore clear that further improvement of the GDL substrate is required in the case of the IBAD electrodes.

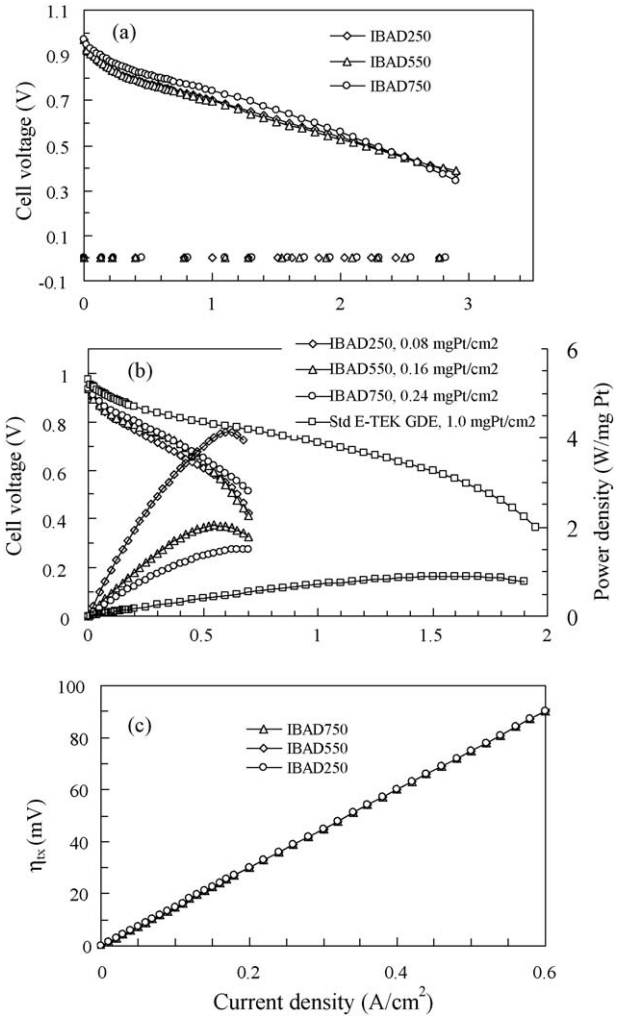

Fig. 6. Performance comparison for IBAD prepared GDE's as a function of Pt loading for (a) H_2/O_2 along with the anode half cell polarizations and (b) H_2/air operation at 80 °C, Nafion® 112 membrane, 50/60 psig anode and cathode back pressure and the stoichiometric ratios (at 1 A/cm^2) were 4.5 H_2 and 3.5 air. MEA Pt loading varied from 0.24 to 0.08 $mg_{Pt(MEA)}$/cm^2 for both anode and cathode electrodes. (c) Mass-transport losses, $\Delta\eta_{tx}$ as a function of current density. The standard E-TEK electrode MEA (1.0 $mg_{Pt(MEA)}$/cm^2) is used for comparison with a standard Nafion® loading of 0.5 mg/cm^2.

Fig. 6 shows the comparison of single cell performance of H_2/O_2 (Fig. 6a), H_2/air (Fig. 6b) for the MEAs made with IBAD250, IBAD550 and IBAD750 anode and cathode, 50/60 psig backpressure for the anode and cathode electrodes, respectively (100% humidification condition) and with a cell temperature of 80 °C. It is quite significant that a low Pt loading of 0.04 mg_{Pt}/cm^2 (IBAD250 cathode) is effective in generating a current density of 1.08 A/cm^2 at a cell voltage of 0.7 V in H_2/O_2 at 80 °C, further in H_2/air such a low loading cathode is effective in reaching a cell voltage of 0.83 and 0.66 V at 0.1 and 0.4 A/cm^2, respectively. This is with the caveat that anode polarization losses are not affected as a function of loading, a fact discernable by comparison of anode polarization curves of IBAD electrodes with 250, 550 and 750 Å corresponding to a loading variation of 0.04–0.12 mg_{Pt}/cm^2, signifying therefore that the difference in polarization is predominantly due to cathode electrode.

Table 2
MEA power densities, P_{MEA} (W/cm^2), Pt-specific power densities, P_{Pt} (g_{Pt}/kW) and gravimetric power density (W/mg_{Pt}) are shown for a series of IBAD electrodes ranging in Pt deposition thickness between 750 and 250 Å corresponding to Pt loading variation in the range of 0.12–0.04 mg_{Pt}/cm^2

Electrode	MEA_{Pt} (mg_{Pt}/cm^2)	P_{MEA} at 0.65 V (W/cm^2)	P_{Pt} at 0.65 V (g_{Pt}/kW)	P_{Pt} at 0.6 V (W/mg_{Pt})
IBAD250	0.08	0.269	0.297	3.862
IBAD550	0.16	0.316	0.506	2.029
IBAD750	0.24	0.327	0.734	1.460
IBAD750P	0.17	0.435	0.386	2.711
Std. E-TEK	1.00	0.845	1.183	0.889

Values from a representative standard Pt/C commercial (E-TEK, De Nora, NJ) electrode (0.5 mg_{Pt}/cm^2) is shown. These values correspond to a cell operating condition of 80 °C, Nafion® 112 membrane, 50/60 psig anode and cathode back pressure, H_2/air and the stoichiometric ratios (at 1 A/cm^2) were 4.5 H_2 and 3.5 air.

The invariance of anode polarization effect is however not dependent on IBAD morphology and has been reported earlier for conventional Pt/C electrocatalyst electrodes where loading as low as 0.05 mg_{Pt}/cm^2 has been reported to be sufficient [48].

Comparison of polarization curves in H_2/air at 80 °C fully humidified conditions, all other parameters being the same as those described earlier (Fig. 6b), shows a variation of power density as a function of IBAD loading. A comparison with Pt/C is also shown. The power density (in W/cm^2) is progressively lower for a concomitant lowering of loading in the IBAD morphology. This corresponds to a decrease of 17% (Table 2) for a three-fold lowering of loading. However, the gravimetric power density (W/mg_{Pt}) exhibits an increase of four-fold when comparing Pt/C conventional electrode versus IBAD 250 at 0.6 V (Fig. 6b and Table 2). This significance can be better illustrated by comparing Pt-specific power density for the IBAD MEA, which is reduced to 0.297 g_{Pt}/kW at 0.65 V using IBAD250 electrode (0.08 $mg_{Pt(MEA)}$/cm^2), a value very close to the automotive target value of <0.2 g_{Pt}/kW. However, the drawback of the IBAD MEA is a simultaneous reduction of MEA area specific power density due to significantly higher mass transport polarization losses. This is illustrated in Table 2, however it is interesting to note that the mass transport contribution variation among the IBAD electrodes does not change significantly as shown in Fig. 6c, hence variations in Pt loading is the principal contributor to the variation in the mass specific power density.

The *iR*-corrected Tafel plots are presented in Fig. 7, this shows that a lowering of Pt loading from 0.12 to 0.04 mg_{Pt}/cm^2 results in a change of *iR*-corrected potential of ≈20 mV, which is in agreement with the expectation based on Eq. (4). This expected outcome is based on a comparison of Pt surfaces with similar morphology unlike the previous comparison (Fig. 5) where a Pt/C was compared with IBAD750. This expected change in the activation overpotential indicates that the electrocatalyst utilization is similar in all the IBAD electrodes, as this outcome is central to this underlying factor.

Since the mass transport overpotential losses are the most crucial aspect of IBAD electrode performance, an attempt was made using a patterned geometry for mitigating this. The beneficial effect of a simply devised pattern design is clearly seen in Fig. 8 where a direct comparison of the fuel cell performance is made between the MEA prepared with IBAD750 (0.12 mg_{Pt}/cm^2) and one prepared with the patterned IBAD750 (IBAD750P) having Pt loading of 0.084 mg_{Pt}/cm^2. Since this technique is based on a deposition process, a simple mask served as a convenient method to enable patterning. Several patterns were attempted, and Fig. 8 shows the representative behavior for an electrode with 30% void spaces (or 70% Pt deposit). Therefore an IBAD750P denotes an electrode with 750 Å thick deposits on 70% of the GDL substrate (LT1400, E-TEK), resulting in an electrode with 0.084 mg_{Pt}/cm^2 instead of 0.12 mg_{Pt}/cm^2. The geometry used in the pattern in the present case was hexagons, however a multitude of different geometric shapes can be considered. Comparison of polarization curves in H_2/O_2, H_2/air are shown in Fig. 8a and b. As evident from the polarization curves in Fig. 8a, with H_2/O_2, very little variation is observed for all the three polarization losses (activation, ohmic and mass transport). This is expected as the only difference in the two MEA's is the existence of 30% void for the patterned sample. However in the more demanding H_2/air case the beneficial effect of patterning (Fig. 8b) is observed. The relative contribution of the corresponding mass transport polarization losses is shown in Fig. 8c. Here at a current density of 600 mA/cm^2 (approximately at 0.6 V for IBAD750), there is a decrease in mass transport contributions by 30% (Fig. 8c). Alternatively, at a cell voltage of 0.6 V current density of 0.575 and 0.775 A/cm^2 were obtained for IBAD750 and IBAD750P, respectively. Operating conditions for the cell was the same, i.e., cell temperature of 80 °C, H_2/air. The corresponding power densities were 1.460 W/mg_{Pt} (IBAD750) and

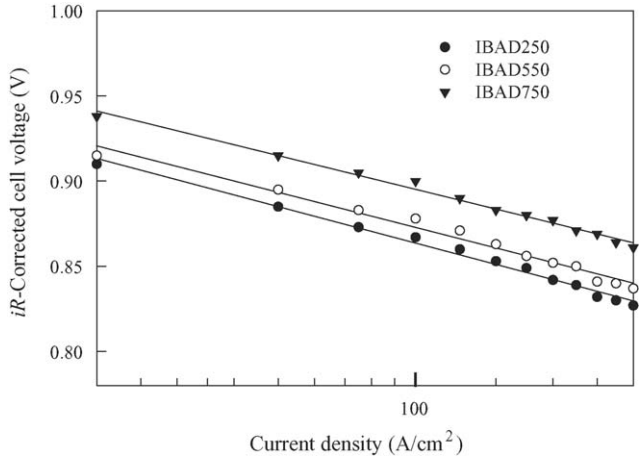

Fig. 7. *iR*-corrected Tafel plots for oxygen reduction on IBAD GDEs in proton exchange membrane fuel cells, 80 °C, 50/60 psig anode and cathode back pressure. MEA Pt loading varied from 0.24 to 0.08 $mg_{Pt(MEA)}$/cm^2 for both anode and cathode electrodes.

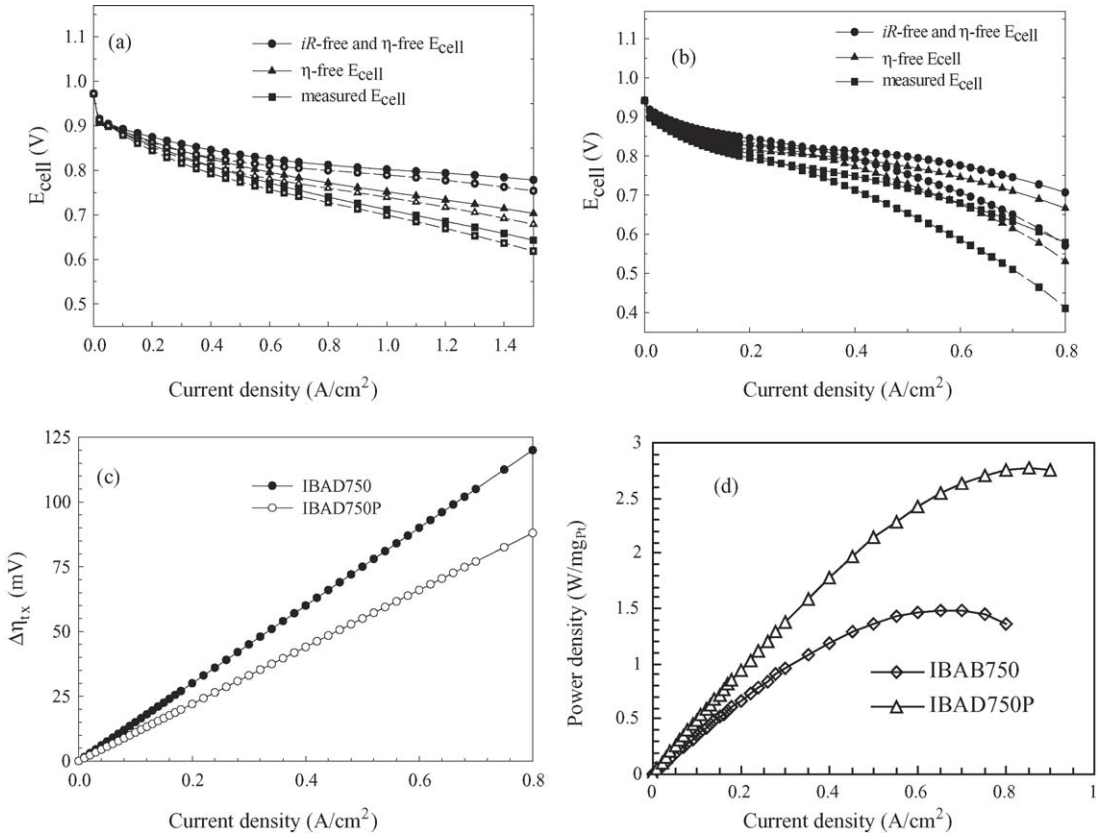

Fig. 8. Comparison of cell performance between the MEA's made using (- - -) IBAD750 and (—) IBAD750P GDE (70% Pt deposit coverage) as anode and cathode electrodes for (a) H_2/O_2 and (b) H_2/air operation at 80 °C, Nafion® 112 membrane, 50/60 psig anode and cathode back pressure and the stoichiometric ratios (at 1 A/cm^2) were 4.5 H_2 and 3.5 air. (c) Comparison of mass-transport losses, $\Delta\eta_{tx}$ and (d) mass specific power density (W/mg$_{Pt(MEA)}$) as a function of current density. Note that the standard MEA loading for 750 Å deposit is 0.24 mg$_{Pt(MEA)}$/cm^2, a 70% coverage electrode constitutes a further approximate lowering in Pt loading to 0.168 mg$_{Pt(MEA)}$/cm^2.

2.711 W/mg$_{Pt}$ (IBAD750P) at 0.6 V (Table 2). This is also illustrated in Fig. 8d, where better mass transport characteristics for the IBAD750P electrode is evident beyond a current density of 0.4 A/cm^2. This particular effect might be pointing to a better gas/liquid diffusivity of the patterned IBAD GDE.

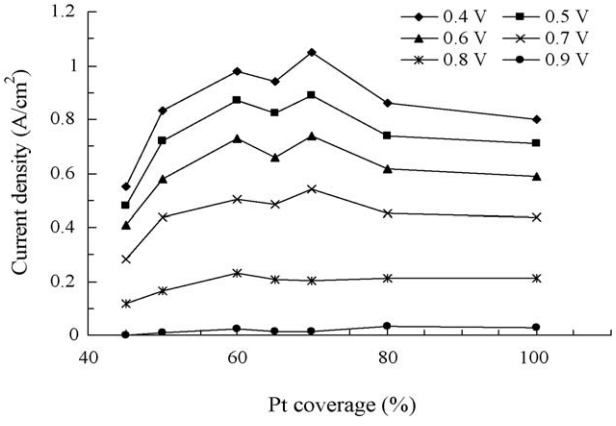

Fig. 9. Variation of current density at different cell voltages as a function of percentage Pt coverage. Cell operating conditions were H_2/air, 80 °C, 50/60 psig anode and cathode back pressure, Nafion® 112 membrane and the stoichiometric ratios (at 1 A/cm^2) were 4.5 H_2 and 3.5 air.

Summary of results on a wide range of patterned samples are shown in Fig. 9. Here performance is compared for MEA's with Pt coverage variations in the range of 45–100%. Current densities at various operating potentials are compared for single cells at 80 °C in H_2/air (standard operating condition). As evident from Fig. 9, the deviations in the current density are observed at potentials below 0.7 V. Further there were spikes towards higher current densities which were observed for 60 and 70% coverage samples. The 70% covered sample constituted the best pattern in the present geometry used (hexagons).

4. Conclusions

Dual IBAD was successfully used to prepare ultra-low Pt loaded gas diffusion electrodes for PEMFC's with the principal advantages of higher mass specific power density (mg$_{Pt}$/kW) combined with the mass manufacturability. Taking the current state of the art Pt/C electrode (E-TEK, De Nora, NJ) with 0.5 mg$_{Pt}$/cm^2 as the control electrode, it was found that mass specific power density of 0.297 g$_{Pt}$/kW was possible with an ultra-low loading IBAD electrode containing 250 Å deposit (0.04 mg$_{Pt}$/cm^2 for a total MEA loading of 0.08 mg$_{Pt}$/cm^2). Among the three different IBAD electrodes reported in this investigation (ranging from 750 to 250 Å deposit corresponding

to 0.04–0.12 mg_{Pt}/cm^2), the mass specific power density variations were 0.29–0.55 g_{Pt}/kW. All these power density comparisons are predicated on a fixed potential of 0.65 V. This is contrasted with the commercial MEA with a loading of 1 $mg_{Pt(MEA)}/cm^2$ where mass specific power density obtained was 1.18 g_{Pt}/kW, a value typical of current state of the art commercial electrodes containing Pt/C. Considering the need to transition from the current state of the art towards a target of 0.2 g_{Pt}/kW, this is a good step forward. However, the principal shortcoming of this effort is the area specific power density which is in the range of 0.27–0.43 W/cm^2 at 0.65 V, hence much below the target value of 0.8–0.9 W/cm^2 (at 0.65 V). The principal cause of this lower area specific power density is the higher mass transport losses. An attempt to mitigate these losses is reported with the use of patterning. In this context a series of patterns ranging from 45 to 80% Pt coverage were used in conjunction with a hexagonal hole geometry. Up to 30% lowering of mass transport losses were realized. Best results were obtained with 70% Pt coverage and were effective below a cell operating potential of 0.7 V. The dual IBAD approach as shown in this investigation is one in which two ion beams were used, one to roughen the substrate and the other to embed the target atoms (Pt in this case). The morphologies obtained are very different from the conventional Pt/C electrocatalyst. Depending on the thickness of the deposit, various levels of crystallinity are obtained. Some differences were observed in the onset potential of CO_{ads} stripping which could be correlated with changes in crystalline nature of the deposit, however a corresponding change in ORR activation polarization was not observed. Instead the change in the ORR, overpotential followed the expected shifts based on Pt loading. The effect of CO_{ads} stripping and its possible correlation with onset potential of water activation needs further investigation. Future efforts also include a careful evaluation of durability of these deposits as compared to the conventional Pt/C electrodes. In an overall sense this constitutes a major advancement in the mass manufacturability of PEM fuel cell electrodes with the promise of achieving ultra-low Pt loading.

Acknowledgements

This work has been sponsored in part by the Department of Energy grant DE-FC04-02AL67606 and it is registered with the Office of Patents and Trademarks under the following numbers: 6,077,621; 6,673,127; 6,017,650 and 6,103,077. The authors wish to gratefully thank Dr. Nazih Hakim (Northeastern University, Boston, MA) for his collaboration in taking the SEM micrographs, Dr. Enrico Ramunni (De Nora Tecnologie Elettrochimiche S.r.l.; Milano, Italy) and Dr. Emory S. De Castro (*E-TEK* Division of De Nora North America, Inc. Somerset, NJ) for their constructive observations during various phases of the project.

References

[1] S. Srinivasan, O.A. Velev, A. Parthasarthy, D.J. Manko, A.J. Appleby, NASA Conf. Publ. 3125 (1991) 101.
[2] S.D. Fritts, R. Gopal, J. Electrochem. Soc. 140 (1993) 3337.
[3] A.J. Appleby, J. Power Sources 37 (1992) 223.
[4] K.B. Prater, J. Power Sources 51 (1994) 129.
[5] K. Kordesch, G. Simader, Fuel Cells and their Applications, VCH, Germany, 1996.
[6] S. Srinivasan, E.A. Ticianelli, C.R. Derouin, A. Redondo, J. Power Sources 22 (1988) 359.
[7] S. Srinivasan, in: O.J. Murphy, B.E. Conway (Eds.), Electrode Kinetic and Electrocatalytic Aspects of Electrochemical Energy Conversion, Plenum Press, New York, 1992, p. 585.
[8] S. Srinivasan, E.A. Ticianelli, C.R. Derouin, A. Redondo, J. Power Sources 22 (1988) 359.
[9] A.C. Ferreira, S. Srinivasan, Proc. Electrochem. Soc. 94 (23) (1994) 173.
[10] H.A. Gasteiger, S.S. Kocha, B. Sompalli, F.T. Wagner, Appl. Catal. B: Environ. 56 (2005) 9.
[11] N.M. Markovic (Ed.), The Hydrogen Electrode Reaction and Electrooxidation of CO and H_2/CO Mixtures on Well Characterized Pt and Pt-bimetallic Surfaces, Handbook of Fuel Cells: Fundamentals, Technology and Applications, vol. 3, Wiley, Chichester, UK, 2003.
[12] M.S. Wilson, S. Gottesfeld, J. Appl. Electrochem. 22 (1992) 1.
[13] Y.G. Chun, C.S. Kim, D.H. Peck, D.R. Shim, J. Power Sources 71 (1998) 174.
[14] M.S. Wilson, S. Gottesfeld, J. Electrochem. Soc. 139 (1992) L28.
[15] L. Xiong, A. Manthiram, Electrochim. Acta 50 (2005) 3200.
[16] Z. Qi, A. Kaufman, J. Power Sources 113 (2003) 37.
[17] M. Uchida, Y. Fukuoka, Y. Sugawara, H. Ohara, A. Ohta, J. Electrochem. Soc. 145 (1998) 3708.
[18] J.C. Figueroa, WO Patent 2,005,008,814 (2005).
[19] T. Yamafuku, K. Totsuka, S. Hitomi, H. Yasuda, M. Yamachi, GS News Tech. Rep. 63 (2004) 23.
[20] R. Mosdale, M. Wakizoe, S. Srinivasan, Proc. Electrochem. Soc. 94 (23) (1994) 179.
[21] G.S. Kumar, S. Parthasarathy, IN Patent 93-MA264 181963 (1998).
[22] Z.-G. Shao, B.-L. Yi, J.-R. Yu, Dianhuaxue 6 (2000) 317.
[23] N. Tsumura, S. Hitomi, H. Yasuda, M. Yamachi, GS News Tech. Rep. 62 (2003) 21.
[24] E.J. Taylor, E.B. Anderson, N.R.K. Vilambi, J. Electrochem. Soc. 139 (1992) L45.
[25] E.J. Taylor, M.E. Inman, WO Patent 2,000,028,114 (2000).
[26] O. Antoine, R. Durand, Electrochem. Solid-state Lett. 4 (2001) A55.
[27] B.N. Popov, Plating Surf. Finish. 91 (2004) 40.
[28] S. Mukerjee, S. Srinivasan, A.J. Appleby, Electrochim. Acta 38 (1993) 1661.
[29] S. Hirano, J. Kim, S. Srinivasan, Electrochim. Acta 42 (1997) 1587.
[30] S.Y. Cha, W.M. Lee, J. Electrochem. Soc. 146 (1999) 4055.
[31] A.T. Haug, Ph.D. Thesis, 2002, p. 185.
[32] C.K. Witham, W. Chun, T.I. Valdez, S.R. Narayanan, Electrochem. Solid-state Lett. 3 (2000) 497.
[33] C.K. Witham, T.I. Valdez, S.R. Narayanan, Proc. Electrochem. Soc. 4 (2001) 114.
[34] N. Cunningham, E. Irissou, M. Lefevre, M.C. Denis, D. Guay, J.P. Dodelet, Electrochem. Solid-state Lett. 6 (2003) A125.
[35] M.K. Debe, T.N. Pham, A.J. Steinbach, US Patent 97,948,851 (1999).
[36] M.K. Debe, R.J. Poirier, M.K. Wackerfuss, R.J. Ziegler, US Patent 97,948,599 (1999).
[37] M.K. Debe, G.M. Haugen, A.J. Steinbach, J.H. Thomas, R.J. Ziegler, US Patent 5,879,827 (1999).
[38] M. K. Debe, J.M. Larson, W.V. Balsimo, A.J. Steinbach, R.J. Ziegler, US Patent 97,948,627 (1999).
[39] J.K. Hirvonen, Mater. Res. Soc. Symp. Proc. 792 (2004) 647.
[40] T. Hoshino, K. Watanabe, R. Kometani, T. Morita, K. Kanda, Y. Haruyama, T. Kaito, J. Fujita, M. Ishida, Y. Ochiai, S. Matsui, J. Vac. Sci. Technol. B: Microelectron. Nanometer Struct.: Process. Measur. Phenom. 21 (2003) 2732.
[41] D.A. Kotov, Rev. Sci. Instrum. 75 (2004) 1934.

[42] A.F. Gulla, M.S. Saha, R.J. Allen, S. Mukerjee, Electrochem. Solid-state Lett. 8 (2005) A504.
[43] R.J. Allen, J.R. Giallombardo, US Patent 6,077,621 (2000).
[44] C.A. Cavalca, J.H. Arps, M. Murthy, US Patent 6,300,000 (2001).
[45] M.G. Fernandes, D.A. Thompson, W.W. Smeltzer, J.A. Davies, J. Mater. Res. 5 (1996) 98.
[46] H.N. Dinh, X. Ren, F.H. Garzon, P. Zelenay, S. Gottesfeld, J. Electroanal. Chem. 491 (2000) 222.
[47] C. Bock, M.-A. Blakely, B. MacDougall, Electrochim. Acta 50 (2005) 2401.
[48] H.A. Gasteiger, J.S. Panels, S.G. Yan, J. Power Sources 127 (2004) 162.